Fast and Slow Response to Global Warming: Sea Surface Temperature and Precipitation Patterns

Shang-Min Long[1*], Shang-Ping Xie[1, 2], Xiao-Tong Zheng[1], Qinyu Liu[1]

1. Key Laboratory of Physical Oceanography, Ministry of Education and Key Laboratory of Ocean-Atmosphere Interaction and Climate in Universities of Shandong, Ocean University of China, China

2. Scripps Institution of Oceanography, University of California at San Diego, La Jolla, California 92093, USA

*Corresponding author address: Shang-Min Long, College of Physical and Environmental Oceanography, Ocean University of China, 238 Songling Road, Qingdao, Shandong 266100, China.

Email: smlong4861@gmail.com

Abstract

The time-dependent response of sea surface temperature (SST) to global warming and the associated atmospheric changes are investigated based on a 1% year^{-1} CO_2 increase to quadrupling experiment of the Geophysical Fluid Dynamics Laboratory climate model version 2.1. The SST response consist of a fast component for which the ocean mixed layer is in quasi-equilibrium with the radiative forcing, and a slow component due to the gradual warming of the deeper ocean in and beneath the thermocline. A diagnostic method is proposed to isolate spatial patterns of the fast and slow response. The deep ocean warming retards the surface warming in the fast response but turns into a forcing for the slow response. As a result, the fast and slow responses are nearly opposite to each other in spatial pattern, especially over the subpolar North Atlantic/Southern Ocean of the deep/bottom water formation, and in interhemispheric SST gradient between the southern and northern subtropics. Wind-evaporation-SST feedback is an additional mechanism for the SST pattern formation in the tropics. Analyses of a Coupled Model Intercomparison Project Phase 5 (CMIP5) multi-model ensemble of global warming simulations confirm the validity of the diagnostic method that separates the fast and slow response. Tropical annual rainfall change follows the SST warming pattern both in the fast and slow response in CMIP5, increasing where the SST increase exceeds the tropical mean warming.

1. Introduction

The increase in atmospheric concentrations of CO_2 and other greenhouse gases (GHGs) impacts the climate system significantly. Ocean plays a major role in determining the warming rate induced by GHGs and shaping its spatial pattern (Hoffert et al. 1980; Bryan et al. 1982, 1988; Thompson and Schneider 1982; Harvey and Schneider 1985; Schlesinger et al. 1985; Stouffer et al. 1989; Power and Hirst 1997, Manabe and Stouffer 2007). The climate response to the radiative forcing is delayed by ocean due to its enormous heat capacity. Meanwhile, the heat absorbed by ocean prolongs the warming effect on climate.

Although GHG increase is nearly uniform in space, pronounced spatial variations emerge in sea surface temperature (SST) response. The magnitude of spatial deviations is as large as the tropical-mean value (Xie et al. 2010). Furthermore, tropical annual rainfall changes follow the pattern of SST warming, consistent with the hypothesis that rainfall increases where SST warming exceeds the tropical mean value (Xie et al. 2010; Lu et al. 2012; Chadwick 2013a). Chadwick et al. (2013a) analyzed tropical precipitation and atmospheric circulation changes in models of Coupled Model Intercomparison Project Phase 5 (CMIP5) (Taylor et al. 2012) and pointed out that part of the dynamical contribution (the weakening circulation) opposes the thermodynamic contribution to tropical rainfall change, rendering the SST warming pattern effect prominent. The SST pattern is also found to be important in explaining both the multi-model ensemble mean distribution and inter-model variability of rainfall change (Ma and Xie 2013). Observations suggest that the Walker circulation slowdown for the past six decades is driven by SST warming pattern of the tropical Indo-Pacific Oceans (Tokinaga et al. 2012). Modest changes in the tropical Pacific may impact the global climate prominently (Karnauskas et al. 2009).

Wind-evaporation-SST (WES) (Xie and Philander 1994) feedbacks is important for the tropical SST pattern (Xie et al. 2010, Lu et al. 2012). In the extratropics, ocean heat transport is influential on SST pattern formation mainly through ocean circulation change (Xie et al. 2010). The dominant mechanism for temperature pattern may differ at different stages of global

warming. Over the tropical Pacific, surface heat flux adjustments dominate the surface warming pattern during the transient stage, while horizontal advection is more important during the equilibrium stage (Yang et al. 2009). Indeed, the slow evolution of ocean currents and the thermohaline circulation in response to global warming may lead to a time-varying spatial distribution in surface warming that differs from the equilibrium response (Manabe et al. 1991). This study examines the time-dependent response of SST with a focus on ocean dynamics effects.

Global-mean surface air temperature (SAT) response to radiative forcing shows clearly short and long timescales in the atmosphere-ocean general circulation models (Olivié et al. 2012). For an abrupt CO_2 doubling, the global-mean SST displays at least two prominent timescales: the fast response of the ocean mixed layer (OML) and the slow response of the deeper ocean (Dickinson 1981; Manabe et al. 1990). The timescale of the former is several years, while the latter is hundreds of years or longer (Stouffer 2004). Jarvis (2011) revealed a third shorter timescale to the ocean response of just over 1 year that regulating the global-mean surface temperature in climate model. Note that fast and slow responses in the ocean are different from those in the atmosphere (Andrews et al. 2010).

Held et al. (2010) isolate the fast and slow components of global warming experimentally by returning GHG forcing abruptly to the preindustrial level. The response of surface temperature shows an initial fast exponential change (fast component) and leaves behind a residual (slow component) that evolves slowly. The two components display distinct spatial patterns. While successful, this method requires costly numerical experiments using coupled climate models. The formation mechanisms and climate impacts of the spatial patterns of the fast and slow components have not been investigated.

The present study examines the time-dependent response of SST to global warming with a focus on the geographic distribution. The effects of SST pattern on the atmosphere are also investigated. Our study is mainly based on the Geophysical Fluid Dynamics Laboratory (GFDL) climate model version 2.1 (CM2.1) CO_2 quadrupling experiment (1%4xCO_2). We show that

spatial variations in SST slightly decrease after the radiative forcing is stabilized, while the global-mean SST continues to increase. We develop a diagnostic method to divide the evolution of SST into fast and slow response. The method is then applied to the coupled climate model simulations and its validity is confirmed by the agreement with experiment results of Held et al. (2010) and our analysis of Representative Concentration Pathway 4.5 (RCP4.5) extension experiment in CMIP5. The fast and slow response of SST shows distinct patterns and displays opposite zonal-mean and horizontal structures in most oceans. The atmosphere circulation and the deeper ocean are also found to display distinct patterns between the fast and slow response. The pattern formation mechanisms, especially ocean dynamical effects, are investigated. Furthermore, we examine the influences of SST pattern on precipitation in CMIP5 and show that the tropical annual precipitation change follows the SST warming pattern both in the fast and slow response. The present study extends previous ones of fast and slow response with a close look into ocean-atmospheric patterns in space and by developing a method that can be applied diagnostically to any long climate change simulations.

The rest of the paper is organized as follows. Section 2 describes the model simulations. Section 3 discusses the physical basis to isolate the fast and slow response based on the evolution of global-mean response. Sections 4 and 5 present spatial patterns of the surface response and the vertical structure of ocean temperature response, respectively. Sections 6 and 7 analyze the SST responses and its effect on precipitation in CMIP5 multi-model ensemble simulations, respectively. Section 8 is a summary.

2. Models

The output of preindustrial control and 600 year 1%4xCO_2 experiments of CM2.1 is analyzed. In the latter, CO_2 is increased 1% $year^{-1}$ from the preindustrial level to quadrupling at year 140, and held constant thereafter. The atmospheric component, AM2.1, builds on a finite volume atmospheric dynamical core and has a resolution of 2° latitude×2.5° longitude. The ocean component, OM3.1, has a resolution of 1° longitude × 1° latitude with meridional grid spacing decreasing to $^1/_3$° toward the equator. It has 50 vertical levels, 22 of which are in the

upper 220m. The detailed description of CM2.1 is provided by Anderson et al. (2004) and Delworth et al. (2006).

We also use simulations from nine coupled climate models (Table 1) in CMIP5 for a multi-model perspective. These 9 models are selected because their RCP4.5 simulations extend to 2300, long past the radiative forcing stabilization. Both the historical (20th century with all forcing for 1850-2005) and the RCP4.5 (2006-2300, approximately with a radiative forcing of 4.5 $W \cdot m^{-2}$ around year 2100) simulations are used. The spatial resolution varies among models. To facilitate comparison, we interpolated all the model output on to a common grid of 2.5° longitude × 2.5° latitude. For each model only one member run ("r1i1p1") is analyzed.

3. Physical basis and global-mean response

a. Physical interpretation of the fast and slow response

Consider a simple two-box model to help understand in the global-mean SST response on fast and slow timescales (Gregory 2000, Held et al. 2010):

$$c_m \frac{\partial T}{\partial t} = Q - \varepsilon_a T - \varepsilon_o (T - T_D) \qquad for \quad the \quad mixed \quad layer, \quad (1)$$

$$c_d \frac{\partial T_D}{\partial t} = \varepsilon_o (T - T_D) \qquad for \quad the \quad deeper \quad ocean. \quad (2)$$

Here, T is the global-mean SST change, T_D deeper ocean temperature change, Q the imposed climate forcing, ε_a the SST damping rate and ε_o the mixing coefficient between the OML and deeper ocean, c_m and c_d are the heat capacity of the OML and deeper ocean, respectively. The deeper ocean response is much reduced because $c_d \gg c_m$ (Gregory 2000).

A quasi-equilibrium state of the OML can be achieved when a gradual radiative forcing of a timescale longer than the fast OML adjustment time is imposed. For that we can neglect the term involving c_m, and obtain:

$$T \approx \frac{Q}{\varepsilon_a + \varepsilon_o} + \frac{\varepsilon_o}{\varepsilon_a + \varepsilon_o} T_D. \qquad (3)$$

T at any time is the sum of two terms: the fast OML adjustment to radiative forcing change

($T_f = \frac{Q}{\varepsilon_a + \varepsilon_o}$), and the slow evolution of the deeper ocean ($T_s = \frac{\varepsilon_o}{\varepsilon_a + \varepsilon_o} T_D$).

Substituting (3) into (2) yields the slow evolution equation for the deeper ocean:

$$c_d \frac{\partial T_D}{\partial t} = \varepsilon_o (T_f - \frac{\varepsilon_a}{\varepsilon_a + \varepsilon_o} T_D). \qquad (4)$$

The response time scale of the deeper ocean, $c_d \frac{\varepsilon_a + \varepsilon_o}{\varepsilon_a \varepsilon_o}$, is far greater than that of the OML, $\frac{c_m}{\varepsilon_a}$. The equilibrium state of the deeper ocean temperature is achieved when $T = T_D$:

$$T_D^e = T^e = \frac{Q}{\varepsilon_a}. \qquad (5)$$

The deeper ocean warming is mainly through mixing and ventilation, which are represented by ε_o (the mixing coefficient between the OML and deeper ocean). In reality, ε_o varies geographically, e.g. large in upwelling regions (Clement et al. 1996). Large ε_o acts to damp the fast component of the SST response, causes more deeper ocean warming and enhances the slow component, while small ε_o has the opposite effect. As a result, the geographic distribution of ε_o can create spatial variations in SST change.

We consider a simple radiative forcing path way: it gradually increases (t > 0) and then stabilizes at time t_c. In the first epoch, the increase in T is dominated by the fast component. In the second epoch ($t > t_c$), T increases only due to the slow component. Figure 1 shows the temporal variation of the global-mean SST and its fast and slow components, based on the preindustrial control and 1% year^{-1} CO_2 increase to doubling (1%2xCO_2) experiments. In the 1%2xCO_2 run, while CO_2 concentration stabilizes after 70 years, the eventual equilibrium state is achieved in thousands of years (Stouffer 2004). For our two-box model, the equilibrium SST response to CO_2 doubling is chosen to be 2.2 °C, with ε_a = 1.7 W·m^{-2} ·K^{-1} and ε_o = 2

$W \cdot m^{-2} \cdot K^{-1}$. For $t < t_c$, the SST change is mainly due to the fast component $T_f = \frac{Q}{\varepsilon_a + \varepsilon_o}$. For $t > t_c$, the slow component T_s dominates further changes in SST [$T - T(t_c) = \frac{\varepsilon_o}{\varepsilon_a + \varepsilon_o} T_D$]. In the first epoch, the OML heats the deeper ocean and T_D evolves much slowly than T, resulting in an increase in ocean stratification ($T - T_D > 0$). When $t > t_c$, with the stabilization of radiative forcing, T_D warms faster than T, acting to warm SST gradually. As a result, the sign of the heat flux change between the OML and deeper ocean is downward in the first epoch and turns upward in the second epoch. We expect that SST warming will display opposite spatial structures between the two stages due to the sign reversal of the subsurface heat flux change. This transition is especially large where ε_o is large, causing the SST pattern to reverse sign significantly between the two stages.

We adopt a convenient relationship to diagnose the ocean storage/heat transport effect on SST (D_o), which is balanced by the net surface flux to first order: $D_o = -Q_{net}$ (Xie et al. 2010).

b. Global-mean response

Figure 2 displays near global ocean (60°S-60°N) annual mean changes of several variables in the 1%4xCO_2 experiment, referenced to the preindustrial control run in CM2.1. Near global-mean SST (Fig. 2a) displays two distinct rates of growth before and after t_c = 140 year. The transition of SST growth from the fast to slow rate is delayed by a few years relative to the CO_2 concentration stabilization, due to the adjustment time of the OML. Spatial variations of SST warming increase with SST in the fast response but then level off after CO_2 is stabilized, despite a continued increase in SST, indicative of different response processes between the two stages. The slow growth of SST after the CO_2 stabilization results from the heating by the deeper ocean warming.

Along with SST, surface scalar wind speed (Fig. 2b), surface relative humidity and stability (Fig. 2c) all display a clear transition around year 140. Net heat flux (Q_{net}) into ocean increases

with the CO_2 rise for $t < t_c$ and then decreases for $t > t_c$. Near global-mean precipitation follows the trajectory of temperature and the transition at $t = t_c$ is unclear.

c. Diagnostic method

In light of two stages the climate response displays, we propose a diagnostic method to isolate spatial patterns of the fast and slow response. The fast response is evaluated by subtracting the preindustrial climatology from the year 101-150 average in the 1%4xCO_2 run. An additional 10 years after CO_2 stabilization is included due to the delay of the OML response. The slow response is defined as changes after the CO_2 stabilization, computed by subtracting the year 151-200 average from the year 551-600 average in the 1%4xCO_2 run. These time periods for averaging are chosen based on the global-mean response that it is dominant by the fast component when radiative forcing increases and by the slow component when radiative forcing stabilizes. Although the fast and slow components cannot be separated precisely by this method as the fast and slow component timescales may varies with time and regions, the method yields a good approximation at the fast and slow response.

Figure 3 shows the depth-time sections of the near global-mean ocean temperature change. In the total response, the vertical maximum of the ocean warming always appears in the upper ocean. A prominent subsurface maximum (about 50-3000m) warming develops in the slow response (Fig. 3b) where the subsurface warms faster than the upper ocean. Consequently, temperature gradient between the OML and deeper ocean decrease for $t > t_c$ (Xu et al. 2013), consistent with the simple model.

Zonal-mean SST displays opposite structures between the fast and slow response (Figs. 4a, b): regions of enhanced warming appear equatorward of 45°S/N in the fast response but move to higher latitudes in the slow response. We have performed Empirical Orthogonal Function (EOF) analysis of zonal-mean anomalies for the fast and slow response. The pair of the first EOF modes of SST are negatively correlated at -0.58 in space. As discussed in the simple model, the sign reversal of the heat flux change between the OML and deeper ocean contributes to this opposite meridional structure. This opposite structures are especially pronounced in high

latitudes (Fig. 4c) where ocean dynamics/storage, as measured by D_o (Fig. 4d), is important. There, ocean dynamics/storage is a cooling effect and suppresses SST warming for the fast response but turns into a warming effect and intensifies SST warming for the slow response. In the fast response (Fig. 4a), zonal-mean SST features an equatorial peak due to the weak evaporative damping (Liu et al. 2005) and the warming is greater in the northern than southern subtropics due to the WES mechanism (Xie et al. 2010). The latter interhemispheric asymmetry is somewhat opposite in the slow response mainly due to the reversed trade wind change as will be presented later.

4. Global pattern

For convenience, we only show the time difference results for the fast and slow response. They are highly consistent with EOF analyses in spatial patterns (not shown here). Indeed, the fast and slow response patterns we obtain are similar to those obtained by the experimental method of Held et al. (Fig. 7 of Held et al. 2010). Similar regional patterns between these two sets of results include the enhanced equatorial Pacific warming in both the fast and slow spatial patterns, and opposite warming structures between the fast and slow spatial patterns in the southern subtropics in all three ocean basins and Southern Ocean. Both Held et al. (2010) and the present study show the sign reversal of the banded structure in warming in the midlatitude Northern Hemisphere (NH) between the fast and slow spatial patterns. Furthermore, fast response patterns in both these studies display an Indian Ocean dipole (IOD) like warming and slow response patterns display broad reduced warming along the Kuroshio extension. The consistency with Held et al. (2010) validates our diagnostic method of decomposing the SST change into the fast and slow response.

a. Fast response pattern

Figure 5 shows the fast response pattern of SST, D_o, surface wind velocity and scalar wind speed in CM2.1. SST warming displays several pronounced regional patterns that are robust among models in earlier studies, including the enhanced equatorial Pacific warming (Knutson and Manabe 1995; Meehl et al. 2000; Liu et al 2005), subtropical southeast Pacific minimum

(Meehl et al. 2007; Vecchi and Soden 2007a; Lu et al. 2012), and the IOD-like warming in the tropical Indian Ocean (Vecchi and Soden 2007b; Du and Xie 2008; Xie et al. 2010). Besides, the greater warming in the northern than southern subtropics in all three ocean basins, banded structures in the midlatitudes and minimum warming in the Southern Ocean are also consistent with the study of Xie et al. (2010).

In the midlatitude NH, the annual-mean SST warming displays meridional banded structures, which are highly correlated with ocean heat transport (D_o) anomalies: SST warming strengthens where D_o is positive and weakens where D_o is negative (Fig. 5a). In the midlatitude Southern Hemisphere (SH), zonal banded structures of SST are also highly correlated with the change of D_o. In the Southern Ocean and subpolar North Atlantic Ocean where bottom/deep water forms, strong dynamical cooling suppresses SST warming. The correlation between D_o and spatial variations in SST (with the area mean removed) between 60°S and 20°S (20°N and 60°N) is 0.48 (0.58). D_o is also important for SST changes in the tropical Indian Ocean and for the zonal minimum (around 140°W-110°W) in SST over the equatorial Pacific Ocean.

In the SH subtropics, a clear meridional SST minimum (Fig. 5b) is found in all three ocean basins, accompanied by the intensified southeast trades. Both the northeast trades and westerlies weaken in the NH with a slightly weakened Aleutian low, sustaining a warming generally greater than the tropical mean value. The greater warming in the northern than southern subtropics mainly results from the interhemispheric asymmetry of wind speed change. The reduced wind speed in the tropical Atlantic and North Indian Ocean also leads to intensified SST warming, similar to the enhanced warming south of Hawaii where positive ocean heat transport is also favorable for SST increase. The correlation between wind speed change and spatial deviations of SST (with the area mean subtracted) is -0.66 between 25°S and 20°N. Generally, enhanced SST warming follows decreased wind speed change in the tropics and subtropics, and vice versa. This is consistent with previous studies that on the basin scale, wind-evaporation-SST (WES)

mechanism is important in tropical SST pattern formation (Xie et al. 2010; Lu et al. 2012). The reduced SST warming and enhanced wind speed in the subtropics of the SH may be triggered by suppressed SST warming in the high latitudes. Ocean-atmosphere interactions may propagate it to the subtropics by the WES footprinting mechanism (Vimont et al. 2003; Wu et al. 2007; Xie et al. 2010).

b. Slow response pattern

Figure 6 displays the slow response pattern to be compared to the fast response (Fig. 5). The SST warming displays several distinct features from the fast response: the El Niño-like warming in the eastern tropical Pacific, suppressed warming in the equatorial Atlantic and North Indian Oceans, broad reduced warming along the Kuroshio and Kuroshio extension (KE), greater warming in the southern than northern subtropics in all three ocean basins, reversed banded structures in warming in the northern subtropics, and enhanced warming in the Southern Ocean.

Tropical and subtropical SST warming patterns appear to be positively correlated in space with ocean heat transport change over most regions, in contrast with the fast response pattern. Local SST warming and D_o are highly correlated over the midlatitudes in the slow response, especially in the North Atlantic and Southern Ocean. The correlation between D_o and spatial deviations of SST (with the area mean subtracted) in the extratropics south (north) of 20°S (20°N) is 0.71 (0.78), higher than that in the fast response.

Wind speed is reduced in most oceans. The eastern Pacific Ocean north of the equator is an exception where the wind speed increase is collocated with a local minimum warming. The correlation between wind speed change and spatial deviations of SST warming (with the area mean subtracted) between 25°S and 20°N decreases from -0.66 in the fast response to -0.37 in the slow response. Similar to the fast response, wind speed change also contributes to the SST warming pattern formation in the tropics, but with a reduced importance in the slow response.

Atmosphere circulation change is also almost opposite to the fast response. The most pronounced atmosphere circulation change is the deceleration of the southeast trade winds in all

three ocean basins, opposite to the fast response. The enhanced Aleutian low in the slow response is another prominent feature which may be associated with a broad reduced warming in the KE region and enhanced warming in the subpolar North Pacific. Westerly wind anomalies almost disappear in the Southern Ocean, replaced by anomalous easterlies in most longitudes. Similar to the fast response pattern, we speculate that the enhanced warming in the southern subtropics originates from high latitudes via the WES footprint mechanism, especially in the Pacific where dynamical warming suggests an origin from the Southern Ocean (Fig. 6b).

The slow SST response displays a spatial pattern opposite to the fast one in most oceans, explaining why the spatial variations of SST slightly attenuate for $t > t_c$ even though the global-mean SST continues to increase (Fig. 2a). As discussed above, the sign reversal of the heat flux change between the OML and deeper ocean causes the opposite spatial structures between the fast and slow response, especially in regions where ocean dynamical effect is strong. In the subtropics, the reversed trade winds anomalies also contribute to shaping the opposite spatial SST structures between the fast and slow response.

The slow response displays a spatial pattern very different from the fast one, indicative of importance of the deeper ocean evolution. The fast response pattern has been studied in the literature, while the slow response pattern has not been examined because the magnitude of the latter is considerably smaller than former in short simulations (< 100 years). The importance of the slow response pattern, however, will increase as climate evolves toward a new equilibrium, as revealed in the results of the 600 years simulation in CM2.1.

5. Vertical structure of ocean temperature response

Ocean temperature change shows distinct vertical structures between the fast and slow response (Fig. 7). Overall, the warming is surface intensified in the fast response whereas it is hidden below the thermocline in the slow response. The zonal-mean distribution in the upper ocean warming is consistent with the SST warming structures, such as the equatorial warming, asymmetric warming between the northern and southern subtropics and the poleward enhanced warming in the slow response, the last feature extending deep in the vertical due to Southern

Ocean ventilation.

Along the equator (5°S-5°N mean), ocean temperature displays large warming in the upper ocean and small warming in the deeper ocean in the fast response (Fig. 7c), which is almost reversed in the slow response (Fig. 7d). In the fast response, there is a distinct reduced warming/weak cooling along the thermocline in the equatorial Pacific, especially in the western Pacific (the thermocline depth is defined as the depth of the maximum vertical temperature gradient). Westerly wind anomalies in the equatorial Pacific (Fig. 5b) flatten the thermocline (thick blue and red lines in Fig. 7c) and bring up cold thermocline water to suppress the upper warming, consistent with the results of Vecchi and Soden (2007b). This minimum warming in the thermocline is also evident in the eastern tropical Indian Ocean where easterly wind anomalies act to shallow the thermocline. Such a feature is diminished in the equatorial Atlantic. The shoaling thermocline is a major reason for the reduced warming along the thermocline, other factors such as the influence of subtropical ventilation need to be explored.

The thermocline depth change is the combined effect of thermodynamical and dynamical factors. In the fast response, the former generally shoals the thermocline because of surface-intensified warming while the latter acts to flatten the thermocline in the equatorial Pacific. In the slow response, the thermodynamical effect due to enhanced subsurface warming (shaded color in Fig. 7d) offsets the dynamical effect induced by the wind anomalies on the equator, making the thermocline depth change much weaker (thick blue and red lines in Figs. 7c, d). Consistent with Chadwick et al. (2013b), equatorial western Pacific thermocline change appears to follow the wind forcing. In the equatorial eastern Indian Ocean, by contrast, the thermocline slightly deepens in the slow response. The percentage of grid points with increased vertical maximum temperature gradient between 20ºS and 20ºN decreases from 97.49% in the fast response to 67.94% in the slow response, indicating that the temperature gradient between the upper and deeper ocean decreases in some regions. Indeed, the medium thermocline depth change (normalized by global-mean SST change) between 20^{o} S and 20^{o} N decreases from -2.3 $m \cdot K^{-1}$ in the fast response to -0.75 $m \cdot K^{-1}$ in the slow response, suggestive of a

thermodynamical effect on the thermocline as the deeper ocean warms faster than the upper ocean.

6. CMIP5 multi-model ensemble results

Here, we apply the diagnostic method to nine models in CMIP5 RCP4.5 simulations. The fast response is computed by subtracting the average of 1956-2005 (historical run) from the average of 2051-2100, and the slow response by subtracting the average of 2101-2150 from the average of 2251-2300. The RCP4.5 simulations have much weaker radiative forcing (Q ~ 4.5 $W \cdot m^{-2}$ at 2100) than the 1%4xCO_2 run (Q ~ 7.42 $W \cdot m^{-2}$ at year 140). This, along with the difference in the length of integration, causes the spatial distribution and magnitude of climate response to differ between the two experiments. The agreement between the two experiments would indicate the robustness of the diagnostic method.

The CMIP5 ensemble mean results produce fast and slow response patterns of SST (Figs. 12 and 13) that are consistent with the CM2.1 results, including the equatorial warming in the Pacific and Indian Oceans, southern subtropical and Southern Ocean warming, banded structures in warming in the SH. Indeed, the correlation for the fast (slow) SST response pattern (normalized by the tropical man warming) between CM2.1 and CMIP5 is 0.89 (0.57). Furthermore, the correlations of SST (with the area mean subtracted) with D_o and wind speed change are also well produced (Table 2). Specifically, the tropical Indian Ocean SST warming in CMIP5 is highly correlated with ocean heat transport as in the CM2.1 in the fast response. The decreased role of wind speed in the tropical SST pattern formation from the fast to slow response is also evident. The general reversal of the fast and slow response pattern in SST and atmosphere circulation is also produced, especially in the southern subtropics and Southern Ocean. The robust response patterns confirm the utility of the diagnostic method to separate the fast and slow response.

There are some differences between the CM2.1 and CMIP5 results. In CMIP5 fast response, the banded SST warming structures in the North Pacific is less clear, likely due to averaging

across models. A broad enhanced SST warming appears in the high latitude NH accompanies with negative ocean heat transport changes. Major differences in CMIP5 slow response include the weak banded structures in the North Atlantic and reduced minimum warming in the KE region. The enhanced SST warming band in the North Pacific appears farther north in the CMIP5 than in the CM2.1 in the slow response. Besides, the Aleutian low change in the CMIP5 slow response is weak. Generally, disagreements between these two sets of patterns are larger in the NH than in the SH.

7. Precipitation response

Percentage precipitation change (dP/P) in the CMIP5 ensemble shows distinct fast and slow response patterns (Fig. 10) that follow the SST response. In the fast response pattern (Fig. 10a), there is a pronounced band of robust dP/P increase over the equatorial Pacific, anchored by the maximum SST warming. The enhanced warming in the tropical North Indian Ocean causes an increase in dP/P, while the decrease in dP/P is apparently in the southern subtropics associated with the reduced SST warming in all three ocean basins. In the tropical North Atlantic Ocean, the local minimum warming anchors a broad decrease in dP/P. The correlation between the dP/P and relative SST (deviations from the tropical mean) within 20°S-20°N is 0.60.

In the slow response, dP/P increases in the tropical Pacific with the enhanced SST warming, while it decreases over the broad reduced warming in the tropical Western Pacific Ocean (Fig. 10b). The enhanced SST warming in the southern subtropics of all three ocean basins creates clear bands of increase in dP/P. The correlation between dP/P and relative SST (deviations from the tropical mean) within 20°S-20°N is 0.52. Generally, tropical precipitation change is locally positive correlated with relative SST both in the fast and slow response. Rainfall increases (decreases) where SST warming exceeds (falls below) the tropical mean value, indicative of the "warmer-get-wetter" mechanism. The opposite SST warming patterns cause rainfall patterns to be opposite between the fast and slow response. As a result, the rate of increase in spatial variance of annual tropical precipitation slows down from 6.2 $mm \cdot month^{-1} \cdot K^{-1}$ during 2006-2100 when the radiative forcing increases to 5.7 $mm \cdot month^{-1} \cdot K^{-1}$ after the radiative

forcing stabilization. This is an important result since precipitation change is to first order spatially variable.

8. Summary

We have investigated the fast and slow response of SST in global warming and their influences on the atmosphere, mainly based on a 1%4xCO_2 simulation with CM2.1. While global-mean SST continues to increase at a reduced rate after the CO_2 stabilization, spatial variations of the SST warming attenuate. We have developed a diagnostic method, as opposed to Held et al.'s (2010) experimental method, to divide the SST change into two stages and isolate the respective spatial patterns: the fast response where the OML is in quasi-equilibrium with both the atmosphere and deeper ocean, and the slow response where the slow evolution of the deeper ocean gradually heats the OML and atmosphere after radiative forcing stabilizes. We have applied the method to a CMIP5 multi-model ensemble simulation, and obtained spatial patterns of the fast and slow response similar to those from the CM2.1. The consistency between these two sets of results confirms the utility of the method that separates the fast and slow response diagnostically.

Spatial patterns of the fast and slow SST response are distinct. The SST warming pattern tends to be opposite between two stages of the response, especially in regions where ocean dynamical effect is strong. This is due to the sign reversal of the heat flux change between the OML and deeper ocean as indicated by the change in vertical structure of ocean temperature. The deeper ocean retards the SST warming in the fast response, as in the Southern Ocean/North Atlantic bottom/deep water formation region. The deeper ocean reverses to heat the OML in the slow response, an effect most apparent in the above bottom/deep water formation region. The equatorial Pacific is an exception, featuring enhanced warming in both the fast and slow response. There the equatorial peak warming is due to the weak evaporative damping in the fast response (Liu et al. 2005; Xie et al. 2010) whereas it seems to result from the positive upward heat flux change in the slow response (Figs. 6a, 7b, d). Besides ocean dynamic/storage, wind speed change also important for SST pattern formation in the tropics, especially for the fast

response. In the CMIP5 ensemble, spatial variations of SST warming exert an important effect on tropical precipitation in both the fast and slow response, with rainfall increasing (decreasing) where SST warming exceeds (falls below) the tropical mean.

The slow response will become important when CO_2 mitigation is implemented. Chadwick et al. (2013b) conducted coupled experiments to explore spatial patterns of the climate response to CO_2 increase and decrease. Surface temperature changes display a more slow response-like pattern in the CO_2 ramp down compared to the CO_2 ramp up (their Figs. 2c, d), including the El Niño-like warming, intensified southern subtropical and Southern Ocean warming, banded structures in the NH and broad reduced warming along the Kuroshio extension. The difference between the CO_2 ramp up and down (Figs 2e, f and Fig. 4b of Chadwick et al. 2013b) resembles the slow response in spatial pattern (our Fig. 6). The fast component is diminished when radiative forcing first increases and is then reduced back to its origin value. The difference is dominated by the slow component. This is a good example of how the slow response influences the surface warming patterns.

Our study has highlighted the differences in SST pattern between the fast and slow response to global warming. Further investigations into pattern formation dynamics and related atmospheric and oceanic processes are needed. Specifically, that the Southern Ocean dynamic/heat storage effect shifts from reducing to enhancing the local SST warming as the climate evolves from the fast to slow response (Fig. 4). We note that this is associated with a change in cross-equatorial gradient in SST warming between the northern and southern subtropics in a way consistent with a coupled ocean-atmospheric energetics argument (Kang et al. 2008; Fuckar et al. 2013). How the extratropical influence takes place and the WES footprint mechanism mediates this adjustment needs to be examined.

Acknowledgments. We wish to thank Yu Kosaka for data assistance, Haijun Yang, and Gen Li for helpful discussions, and anonymous reviewers for constructive comments. This work is supported by the National Basic Research Program of China (2012CB955600), the NSFC (41106010, 41176006) and the U.S. NSF (ATM-0854365).

References

Anderson, J. L., and Coauthors, 2004: The new GFDL global atmosphere and land model AM2-LM2: Evaluation with prescribed SST simulations. *J. Climate*, **17**, 4641-4673.

Andrews, T., P. M. Forster, O. Boucher, N. Bellouin , and A. Jones, 2010: Precipitation, radiative forcing and global temperature change. *Geophy. Res. Lett.*, **37**, L14701, doi:10.1029/2010GL043991.

Bryan, K., F. G. Komro, S. Manabe, and M. J. Spelman, 1982: Transient climate response to increasing atmospheric carbon dioxide. *Science*, **215**, 56-58.

——, S. Manabe and M. J. Spelman, 1988: Interhemispheric asymmetry in the transient response of a couplded ocean-atmospheric model to a CO_2 forcing. *J. Phys. Oceanogr.*, **18**, 851-867.

Chadwick, R., I. Boutle, and G. Martin, 2013a: Spatial patterns of precipitation change in CMIP5: Why the rich don't get richer in the tropics. *J. Climate***,** doi:10.1175/JCLI-D-12-00543.1, in press.

——, P. L. Wu, P. Good, and T. Andrews, 2013b: Asymmetries in tropical rainfall and circulation patterns in idealised CO_2 removal experiments. *Climate Dyn.*, **40,** 295-316.

Clement, A. C., R. Seager, M. A. Cane, and S. E. Zebiak, 1996: An ocean dynamical thermostat. *J.Climate*, **9,** 2190-2196.

Delworth, T. L., and Coauthors, 2006: GFDL's CM2 global coupled climate models. Part I: Formulation and simulation characteristics. *J. Climate*, **19**, 643-674.

Dickinson, R. E., 1981: Convergence rate and stability of ocean-atmosphere coupling schemes with a zero-dimensional climate model. *J. Atmos. Sci.*, **38,** 2500-2514.

Du, Y., and Xie, S.-P., 2008: Role of atmospheric adjustments in the tropical Indian Ocean warming during the 20th century in climate models. *Geophy. Res. Lett.*, **35**, L08712, 10.1029/2008GL033631

Fuckar, N. S., S.-P. Xie, R. Farneti, E. Maroon, and D.M. W. Frierson, 2013: Influence of the extratropical ocean circulation on the intertropical convergence zone in an idealized

coupled general circulation model. *J. Climate*, doi:10.1175/JCLI-D-12-00294.1, in press.

Gregory, J. M., 2000: Vertical heat transports in the ocean and their effect on time-dependent climate change. *Climate Dyn.*, **16,** 501-515.

Harvey, L. D., and S. H. Schneider, 1985: Transient climate response to external forcing on 10^0-10^4 year time scales. Part I: Experiment with globally averaged, coupled atmosphere and ocean energy balance model. *J. Geophys. Res.*, **90**(D1), 2191-2205.

Held, I. M., and M. Winton, K. Takahashi,T. Delworth, and F. R. Zeng, G. K. Vallis, 2010: Probing the fast and slow components of global warming by returning abruptly to preindustrial forcing. *J. Climate*, **23,** 2418-2427.

Hoffert, M. I., A. J. Callegari, and C. -T. Hsieh, 1980: The role of deep sea storage in the secular response to climate forcing. *J. Geophys. Res.*, **85,** 6667-6679.

Jarvis, A., 2011: The magnitudes and timescales of global mean surface temperature feedbacks in climate models, Earth Syst. Dynam., **2**, 213-221, doi:10.5194/esd-2-213-2011.

Kang, S. M, I. M. Held, D. M. W Frierson, and M. Zhao, 2008: The response of the ITCZ to extratropical thermal forcing: idealized slab-ocean experiments with a GCM. *J. Climate*, **21**, 3521–3532.

Karnauskas, K. B., R. Seager, A. Kaplan, Y. Kushnir, and M. A. Cane, 2009: Observed strengthening of the zonal sea surface temperature gradient across the equatorial Pacific Ocean. *J. Climate*, **22,** 4316-4321.

Knutson, T. R., and S. Manabe, 1995: Time-mean response over the tropical Pacific to Increased CO_2 in a coupled ocean-atmosphere model. *J. Climate*, **8,** 2181-2199.

Liu, Z., 2005: Rethinking tropical ocean response to global warming: The enhanced equatorial warming. *J. Climate*, **18,** 4684-4700.

Lu, J., and B. Zhao, 2012: The role of oceanic feedback in the climate response to doubling CO_2. *J. Climate*, **25**, 7544–7563.

Ma, J., and S. -P. Xie, 2013: Regional patterns of sea surface temperature change: A source of uncertainty in future projections of precipitation and atmospheric circulation. *J. Climate*. **26**,

2482-2501

Manabe, K. Bryan, and M. J. Spelman, 1990: Transient response of a global ocean-atmosphere model to a doubling of atmospheric carbon dioxide. *J. Phy. Oceanogr.*, **20,** 722-749.

——, R. J. Stouffer, M. J. Spelman, and K. Bryan, 1991: Transient responses of a coupled ocean-atmosphere model to gradual changes of atmospheric CO_2. Part I: annual mean response. *J. Climate*, **4,** 785-818.

——, S., and R. J. Stouffer, 2007: Role of ocean in global warming. *J. Meteor. Soc. Japan*, **85B,** 385-403.

Meehl, G. A., W. D. Collins, B. A. Boville, J. T. Kiehl, T. M. L. Wigley, and J. M. Arblaster, 2000: Response of the NCAR Climate system model to increased CO_2 and the role of physical processes. *J. Climate*, **13,** 1879-1898.

——, and Coauthors, 2007: Global climate projections. *Climate Change 2007: The Physical Science Basis*, S. Solomon et al., Eds., Cambridge University Press, 747-845.

Power S. B., and A. C. Hirst, 1997: Eddy parametrization and the oceanic response to idealised global warming, *Clim. Dyn.*, **13**, 417-428.

Olivié, D. J. L., G. P. Peters, and D. Saint-Martin, 2012: Atmosphere response time scales estimated from AOGCM experiments. *J. Climate*, **25,** 7956-7972.

Schlesinger, M. E., W. L. Gates, and Y. J. Han, 1985: The role of the ocean in CO_2-induced climatic warming: Preliminary results from the OSU coupled atmosphere-ocean GCM. *Coupled Ocean-Atmosphere Models*, J. C. J. Nihoul, Ed., Elsevier, 447-478.

Stouffer, R. J., 2004: Time scales of climate response. *J. Climate*, **17,** 209-217.

——, S. Manabe, and K. Bryan, 1989: Interhemispheric asymmetry in climate response to a gradual increase of atmospheric CO2. *Nature*, **342,** 660-662.

Taylor, K. E., R. J. Stouffer, and G. A. Meehl, 2012: An overview of CMIP5 and the experiment design. *Bull. Amer. Meteor. Soc.*, **93**, 485-498.

Thompson, S. L., and S. H. Schneider, 1982: Carbon dioxide and climate: The importance of realistic geography in estimating the transient temperature response. *Science*, **217**,

1031-1033.

Tokinaga, H., S. -P. Xie, C. Deser, Y. Kosaka, and Y. M. Okumura, 2012: Slowdown of the Walker circulation driven by tropical Indo-Pacific warming. *Nature*, **491,** 439-443.

Vecchi, G. A., and B. J. Soden, 2007a: Effect of remote sea surface temperature change on tropical cyclone potential intensity. *Nature*, 450, 1066-1070.

——, and ——, 2007b: Global Warming and the Weakening of the Tropical Circulation. *J. Climate*, **20,** 4316-4340.

Vimont, D. J., J. M. Wallace, and D. S. Battisti, 2003: The seasonal footprinting mechanism in the Pacific: Implications for ENSO. *J. Climate*, **16**, 2668–2675.

Wu, L., Z. Liu, C. Li, and Y. Sun, 2007: Extratropical control of recent tropical decadal climate variability: A relay teleconnection. *Clim. Dyn*., **28**, 99–112.

Xie, S.-P., and S. G. H. Philander, 1994: A coupled ocean-atmosphere model of relevance to the ITCZ in the eastern Pacific. *Tellus*, **46A,** 340-350.

——, C. Deser, G. A. Vecchi, J. Ma, H. Y. Teng, and A. T. Wittenberg, 2010: Global warming pattern formation: Sea surface temperature and rainfall. *J. Climate*, **23,** 966-986.

Xu, L. X., S. -P. Xie, and Q. Y. Liu, 2013. Fast and slow response of the North Pacific Mode Water and subtropical countercurrent to global warming. *J. Ocean Univ. China*, **12** (2), 216-221, DOI: 10.1007/s11802-013-2189-6.

Yang, H. J. F. Y. W., and A. D. Sun, 2009: Understanding the ocean temperature change in global warming: The tropical Pacific. *Tellus*, **61,** 371-380.

TABLE 1. List of nine models from CMIP5 analyzed in this Study

Model	Institution
bcc-csm1-1	Beijing Climate Center, China Meteorological Administration (China)
CNRM-CM5	Centre National de Recherches Meteorologiques (France)
CanESM2	Canadian Centre for Climate Modeling and Analysis (Canada)
GISS-E2-R	NASA Goddard Institute for Space Studies (USA)
GISS-E2-H	
IPSL-CM5A-LR	Institute Pierre-Simon Laplace (France)
IPSL-CM5A-MR	
MIROC-ESM	University of Tokyo, NIES, and JAMSTEC (Japan)
MPI-ESM-LR	Max Planck Institute for Meteorology (Germany)

TABLE 2. Correlations with SST deviations (T^*) from area means: changes in ocean heat transport effect D_o, scalar wind speed W, and percentage precipitation change dP/P in CM2.1 and CMIP5 for the fast and slow response.

Correlation		(T^*, D_o) 60°S-20°S	(T^*, D_o) 20°N-60°N	(T^*,W) 25°S-20°N	(T^*, dP/P) 20°S-20°N
CM2.1	fast	0.48	0.58	-0.66	
	slow	0.71	0.78	-0.37	
CMIP5	fast	0.54	0.59	-0.53	0.60
	slow	0.72	0.64	-0.33	0.52

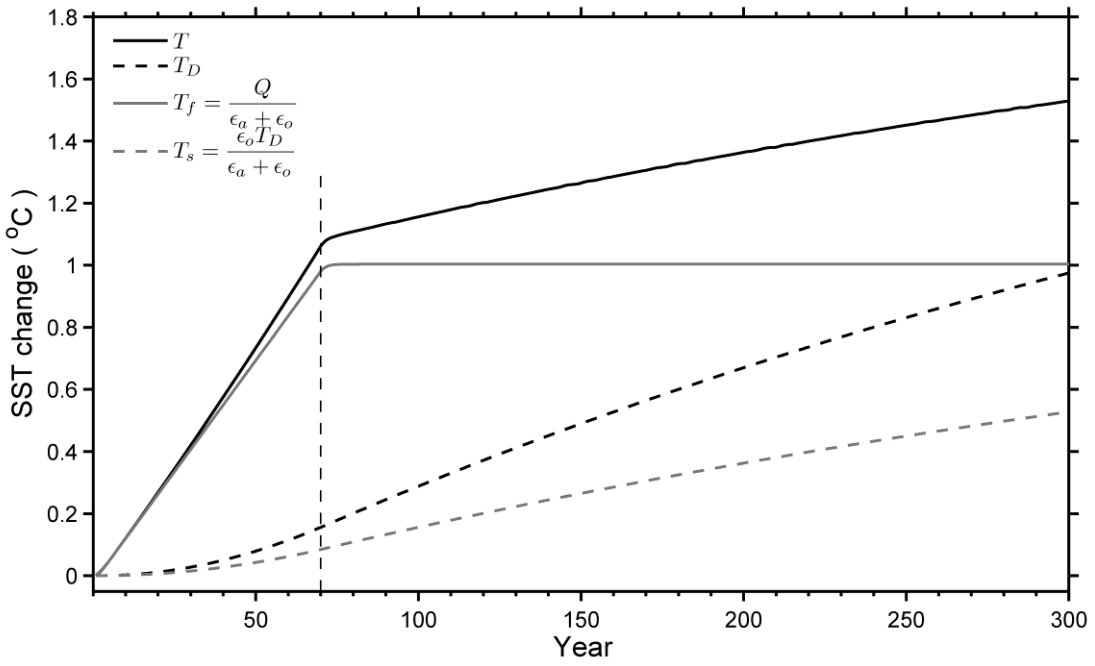

FIG. 1. Schematic for temporal variations of global-mean SST change (°C), its fast and slow components in the 1%2xCO_2 run with respect to the preindustrial control run, with ε_a = 1.7 W·m^{-2} ·K^{-1} and ε_o = 2 W·m^{-2} ·K^{-1}. The thicknesses of the mixed layer and deeper layer are chosen to be 50 m and 3300m, respectively.

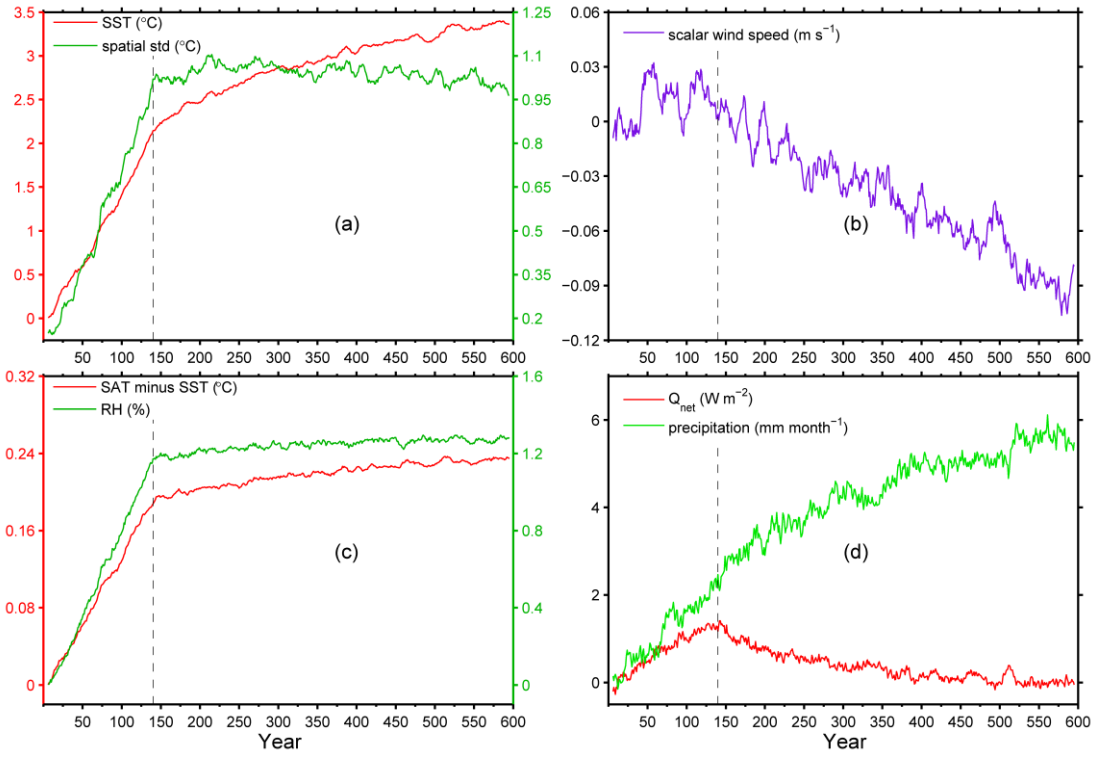

FIG. 2. Evolution of near global ocean (60°S-60°N), annual-mean changes in the 1% 4xCO_2 run with respect to the preindustrial control run in CM2.1: (a) SST (red line, °C) and its spatial standard deviation from the tropical mean value (spatial std, green line, °C); (b) scalar wind speed ($m \cdot s^{-1}$); (c) surface air-sea temperature difference (SAT-SST) (red line, °C) and relative humidity (RH, green line, %); (d) net heat flux Q_{net} (red line, $W \cdot m^{-2}$) and precipitation (green line, $mm \cdot month^{-1}$). In (a) and (c) different colors and scales of the y axis on the two sides are used for different variables. The dotted vertical line stands for the year when the CO_2 concentration reaches quadrupling. 11 years running mean is applied in each panel.

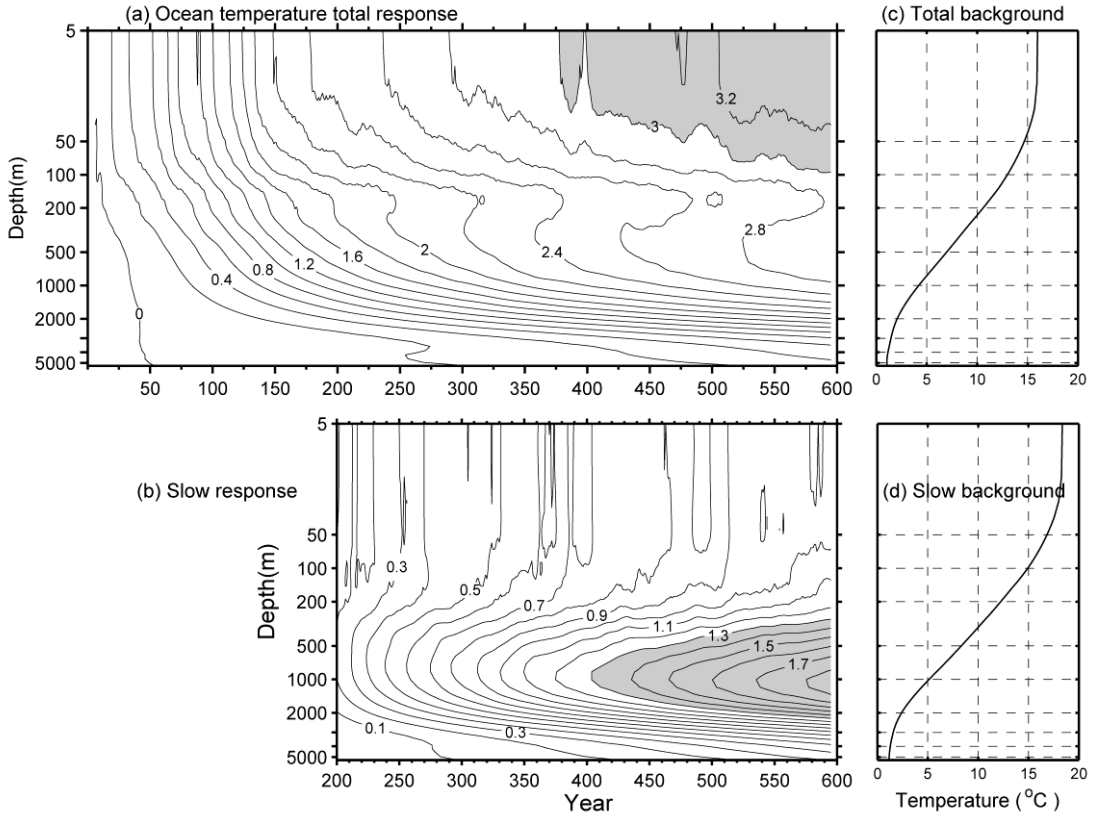

FIG. 3. Time-depth sections of near global (60°S-60°N) mean ocean temperature anomalies (°C) in CM2.1: (a) the total and (b) the slow response. Depth coordinates is on logarithm to highlight the upper ocean, with 11 years running mean applied in each panel. (c) and (d) show the total background temperature (preindustrial climatology) of (a) and the slow background temperature (151-200 mean in 1%4xCO_2) of (b), respectively.

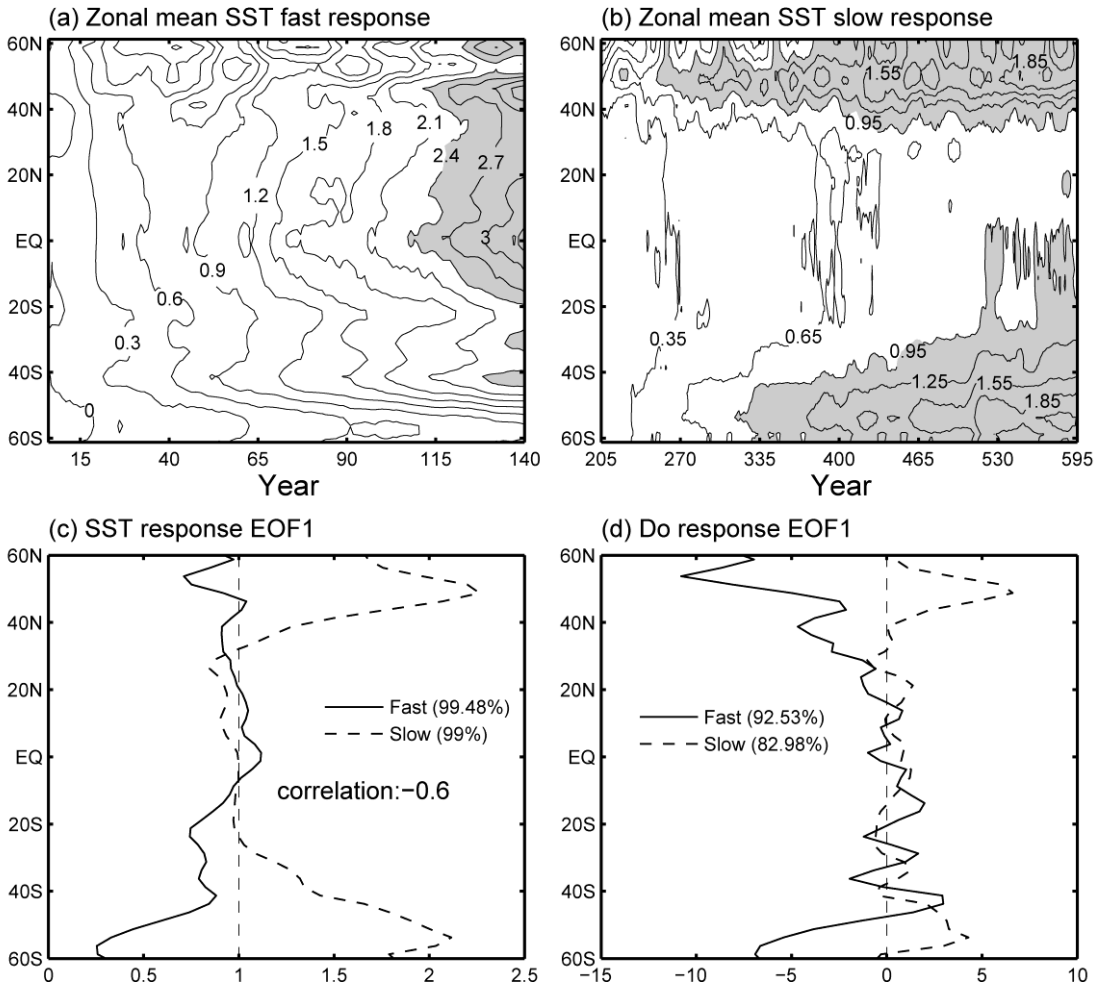

FIG. 4. Time section of zonal-mean SST (°C): (a) the fast and (b) the slow response. First EOF modes (EOF1) of the fast and slow response for: (c) SST and (d) ocean heat transport (D_o), with the first EOF modes of SST normalized by their tropical (20°S-20°N) mean.

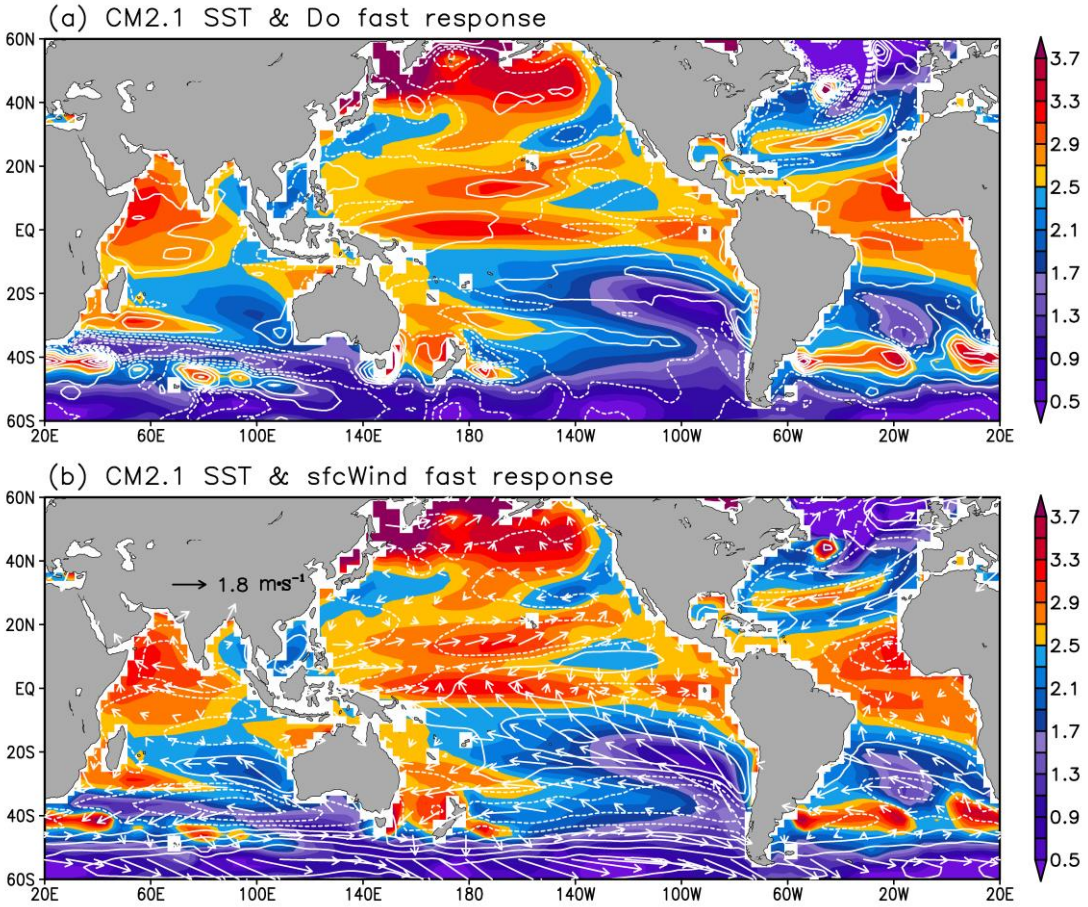

FIG. 5. Annual-mean fast response pattern (year 101-150 mean in the 1%4xCO_2 run minus the preindustrial climatology) in CM2.1: SST [color shaded, °C, with values larger (smaller) than tropical (20°S-20°N) mean shaded by warm (cool) color], along with (a) D_o [white contours, contour interval (CI) 8 $W \cdot m^{-2}$], (b) surface wind velocity (vectors, $m \cdot s^{-1}$) and scalar wind speed (white contours, CI 0.3 $m \cdot s^{-1}$). Zero contours omitted for clarity.

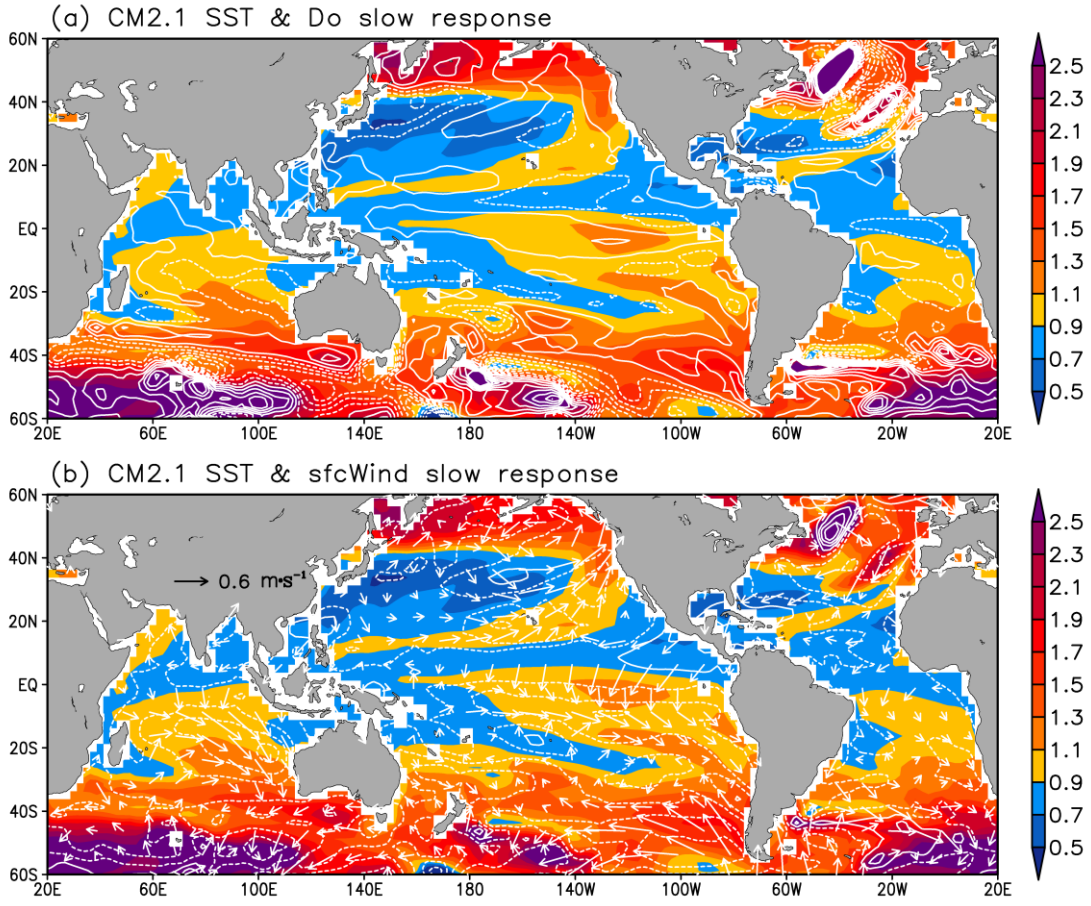

FIG. 6. Annual-mean slow response pattern (year 551-600 mean minus year 151-200 mean in the 1%4xCO_2 run) in CM2.1: SST (color shaded, °C), along with (a) D_o (white contours, CI 4 W·m^{-2}), (b) surface wind velocity (vectors, m·s^{-1}) and scalar wind speed (white contours, CI 0.1 m·s^{-1}). Zero contours omitted for clarity.

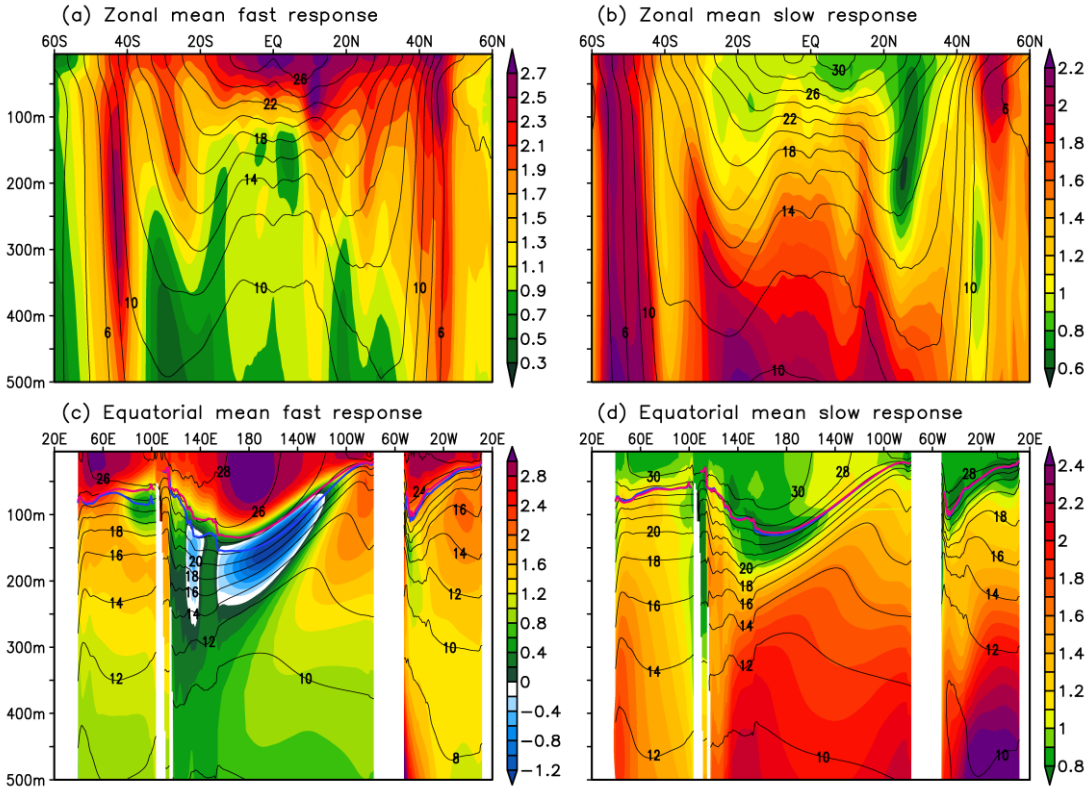

FIG. 7. Vertical structures of ocean temperature change (color shaded, °C) along with background temperature (black contours) in CM2.1: zonal mean (a) fast and (b) slow response; equatorial (5°S-5°N) mean (c) fast and (d) slow response. The thick black and red lines in (c) indicate the thermocline depth of the preindustrial climatology and the year 101-150 mean in 1%4xCO_2, respectively. The thick blue and red lines in (d) indicate the thermocline depth of the year 151-200 mean and the year 551-600 mean in the 1%4xCO_2 run, respectively.

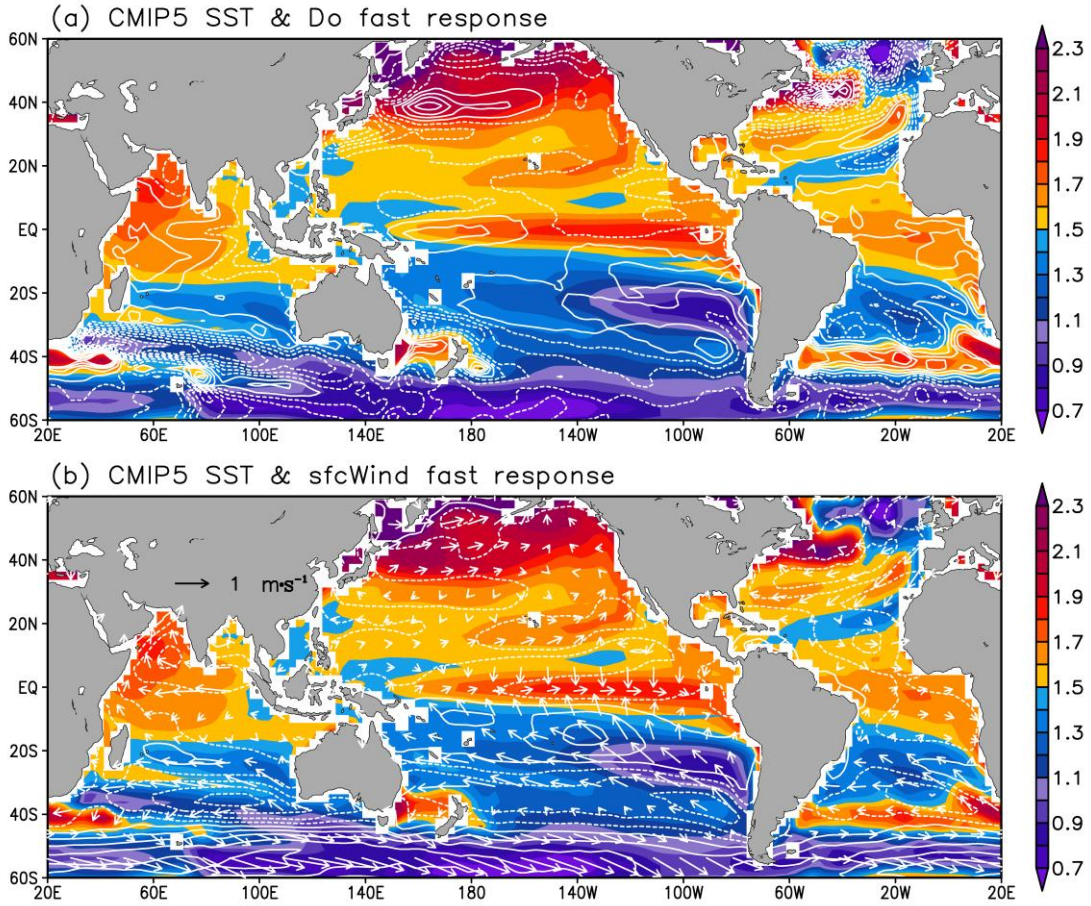

FIG. 8. Annual-mean fast response pattern (2051-2100 mean in RCP4.5 minus 1956-2005 mean in the historical run) in CMIP5: SST (color shaded, °C), along with (a) D_o (white contours, CI 2 $W \cdot m^{-2}$), (b) surface wind velocity (vectors, $m \cdot s^{-1}$) and scalar wind speed (white contours, CI 0.1 $m \cdot s^{-1}$). Zero contours omitted for clarity.

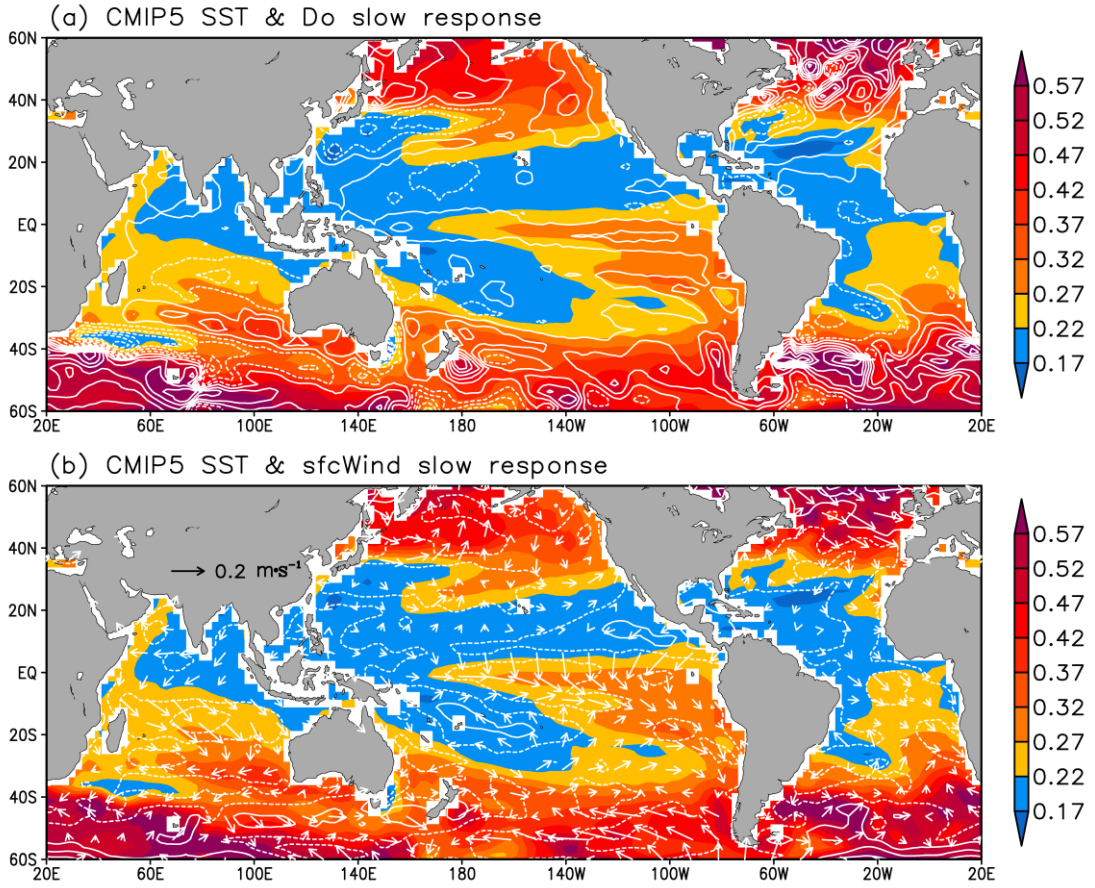

FIG. 9. Annual-mean slow response pattern (2251-2300 mean minus 2101-2150 mean in RCP4.5) in CMIP5: SST (color shaded, °C), along with (a) D_o (white contours, CI 1 W·m^{-2}), (b) surface wind velocity (vectors, m·s^{-1}) and scalar wind speed (white contours, CI 0.03 m·s^{-1}). Zero contours omitted for clarity.

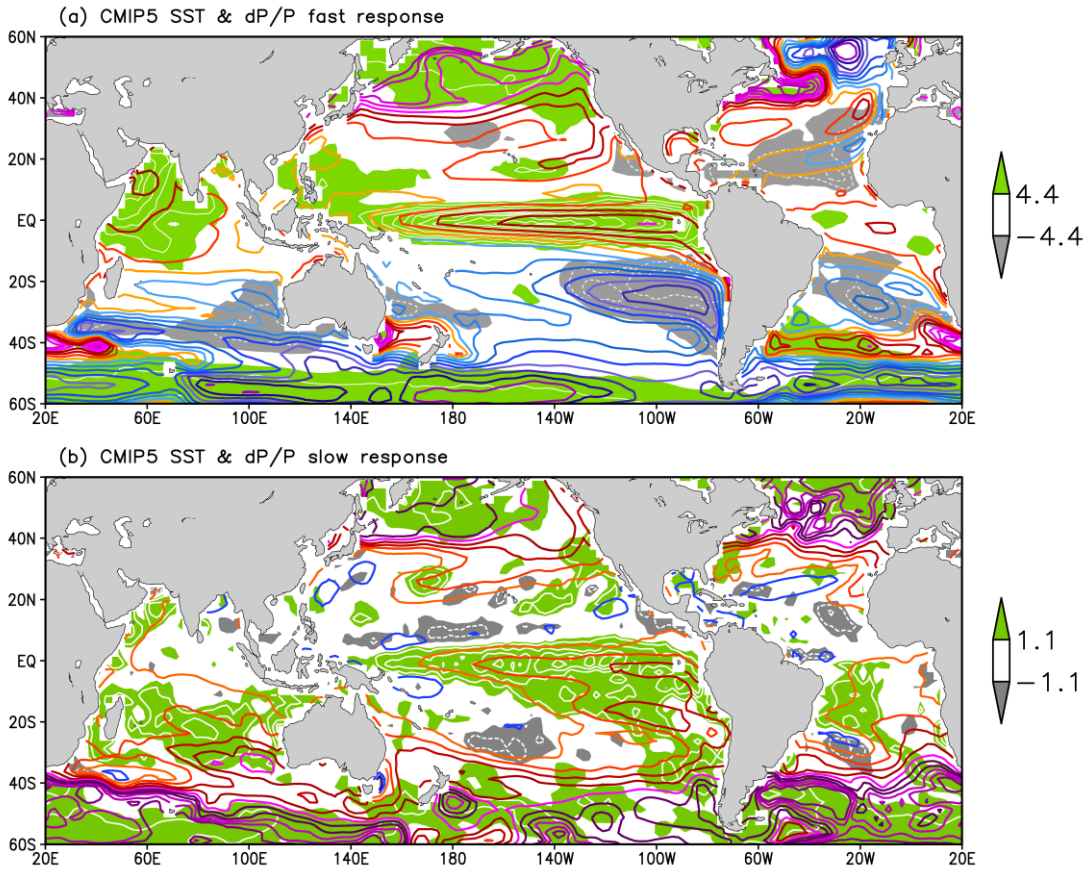

FIG. 10. Percentage precipitation change (dP/P in %, green/gray shade and white contours) along with SST change [contours, °C, with value larger (smaller) than tropical (20°S-20°N) mean contoured by warm (cool) color] in CMIP5 RCP4.5 simulations: (a) the fast response pattern (SST CI 0.1 °C), (b) the slow response pattern (SST CI 0.04 °C). White contour intervals for dP/P change are 4% in (a) and 2% in (b).